JOURNAL OF NANOMATERIALS AND APPLICATIONS

Journal of Nanomaterials and Applications

Journal homepage: https://jna.com.vn

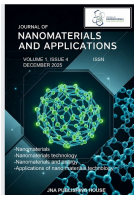

A Temperature and Pressure Sensor Network Application by the Fiber Loop Ringdown Spectroscopy Technique

Burak Malik Kaya [1,*], **Umut Sarac** [2], **Dung Nguyen Trong** [3,*], **Ștefan Țalu** [4]

[1] Eskisehir Osmangazi University, Vocational School of Health Service, 26480, Eskisehir, Türkiye.

[2] Bartın University, Department of Science Education, 74100, Bartın, Türkiye.

[3] University of Transport Technology, Faculty of Applied Science, 54 Trieu Khuc, Thanh Xuan, Hanoi, 100000, Vietnam.

[4] Technical University of Cluj-Napoca, The Directorate of Research, Development and Innovation Management (DMCDI), Constantin Daicoviciu Street, no. 15, Cluj-Napoca, 400020, Cluj county, Romania.

Article info

Type of articles:

Original research paper

Corresponding author*:

Dung Nguyen Trong

E-mail address:

dungnt2018@gmail.com

dungnt78@utt.edu.vn

Received: 27 september 2025

Revised: 26 January 2026

Accepted: 26 January 2026

Published: 28 January 2026

Abstract: A novel sensor network was developed by serially connecting two bare single-mode fiber (SMF) loops without any modification of the sensor heads to simultaneously monitor temperature and pressure variations with high sensitivity and real-time capability using the fiber loop ringdown spectroscopy (FLRDS) technique. Temperature and pressure changes were evaluated based on step-dependent variations in optical loss, which were derived from the recorded ringdown times (RDTs) of each fiber loop. Two fiber loops with lengths of 118±2 m and 43±2 m were employed as temperature and pressure sensors, respectively. The temperature sensor was embedded in a circular copper housing and characterized over the range of 30–150 °C with 30 °C increments, while a cross-point formed in the second loop was utilized as a pressure-sensitive element to measure pressures from 0 to 0.98×10^6 Pa. The sensor network features a simple and optimized architecture, achieving low baseline stabilities of 0.21% for temperature sensing and 0.24% for pressure sensing. To the best of the authors' knowledge, this work represents the first implementation of specially designed bare SMF loops in an FLRDS-based sensor network. Owing to its low cost, compact structure, portability, and high sensitivity, the proposed system is highly promising for applications in healthcare, transportation, and communication

Keywords: fiber loop; FLRDS; pressure sensor; sensor network; temperature sensor

1. Introduction

In recent years, increasing attention has been directed toward the development of multi-parameter optical fiber sensor networks with simplified architectures and high robustness for practical applications.

In particular, sensor systems capable of simultaneously monitoring temperature and pressure using minimal optical components are highly desirable for nano-enabled devices, structural health monitoring, and real-time industrial sensing. However, many reported optical fiber sensing approaches rely on complex sensing heads, wavelength-domain interrogation, or additional optical instruments such as optical spectrum analyzers, which increase system cost, reduce portability, and limit large-scale deployment. Moreover, comparative evaluations focusing on system simplicity, baseline stability, and scalability are often insufficiently addressed. To overcome these limitations, this work introduces a fiber loop ringdown spectroscopy (FLRDS)-based sensor network employing only bare single-mode fiber (SMF) loops for simultaneous temperature and pressure sensing. By eliminating specialized sensing structures and wavelength-domain interrogation, the proposed approach provides a simplified yet highly sensitive and scalable solution. Optical fiber sensors have been widely adopted due to their flexibility, immunity to electromagnetic interference, remote sensing capability, and ease of installation [1–3]. Among various fiber types, SMF offers low signal attenuation, high bandwidth, and long-distance transmission, making it well suited for sensing applications. When combined with the FLRDS technique, SMF-based sensors provide higher sensitivity, lower system cost, fast response, real-time continuous measurement, and improved accuracy compared to conventional approaches [4–8]. Previously reported temperature sensors commonly employ interferometric structures [9–12], fusion-spliced fiber combinations [13,14], fiber Bragg gratings (FBGs) [15–17], or Fabry–Perot cavities [18,19]. Although these sensors exhibit high sensitivity to temperature, pressure, strain, and refractive index (RI), their practical deployment is often limited by fabrication complexity and reproducibility issues. Temperature sensing based on RI variation has also been extensively studied using FP interferometers and FBGs [20–26]. The RI change with temperature is governed by the thermo-optic coefficient, which results from the combined effects of thermal expansion and polarization-induced RI variation in silica fibers, yielding an overall positive RI change [27–29]. For pressure and strain sensing, FLRDS-based systems have been investigated to enhance sensitivity, stability, and repeatability by reducing baseline noise and improving dynamic range [30–33]. In this study, a novel FLRDS sensor network design is presented in which a bare SMF loop itself functions as the temperature sensor without any modification, while a designated region of a second fiber loop serves as the pressure-sensitive element. The sensor network is formed by serially connecting two fiber loops, enabling multi-parameter sensing within a single system. In FLRDS operation, a small portion of the injected optical pulse circulates multiple times within the fiber loop, undergoing exponential decay due to intrinsic optical loss, while a fraction is detected at each round trip. The decay time constant, referred to as the ringdown time (RDT), directly reflects the optical loss, allowing sensitive detection of external perturbations. Most optical temperature sensing studies rely on FBGs or interferometric mechanisms [34–39], both of which require optical spectrum analyzers and are sensitive to light source fluctuations, resulting in higher system cost and reduced stability. Although several FLRDS-based temperature sensing systems have been reported, many still incorporate FBGs, interferometric structures, or multiplexing techniques [40–42]. Multi-parameter sensing studies combining temperature with pressure, strain, displacement, or surface RI have also been demonstrated using various techniques, including SMF–FBG loops [43], birefringent fiber loop mirrors [44], Brillouin scattering [45], wavelength and intensity modulation [46], and Rayleigh scattering [47]. However, the sensing mechanisms, system designs, and required components in these studies differ fundamentally from the present work. In contrast to previously reported FLRDS-based temperature and pressure

sensors that rely on FBGs, interferometric structures, or optical spectrum analyzers, the proposed system achieves comparable sensitivity using a significantly simpler architecture. The exclusive use of bare SMF loops and time-domain ringdown interrogation eliminates the need for complex optical components, resulting in a low-cost, robust, and easily scalable sensor network. Unlike earlier studies [43–47], the present work employs no modified sensing heads or wavelength-domain instruments. Building upon prior investigations [48,49], this study represents the first demonstration of an FLRDS-based sensor network capable of simultaneously measuring temperature and pressure using only bare single-mode fiber loops. To the best of the authors' knowledge, this is the first FLRDS-based sensor network that simultaneously measures temperature and pressure using only bare single-mode fiber loops, without any wavelength-domain interrogation or modified sensing heads. Beyond its sensing performance, the proposed FLRDS network is highly relevant to nano-enabled and advanced material systems. The bare SMF acts as an intrinsic sensing medium, where evanescent-field interaction and refractive-index modulation occur at sub-micrometer length scales comparable to nanomaterial dimensions. This enables straightforward integration with nano-coatings, nanocomposites, or nanostructured surfaces, providing a scalable platform for future nano-functionalized fiber sensors. The combination of low baseline stability, multi-parameter capability, system simplicity, and time-domain interrogation distinguishes the proposed approach from existing FLRDS and fiber-optic sensor systems, making it highly attractive for medical, structural health monitoring, chemical, biological, and physical sensing applications requiring fast response, high sensitivity, and real-time operation.

2. The network system setup and the FLRDS principle

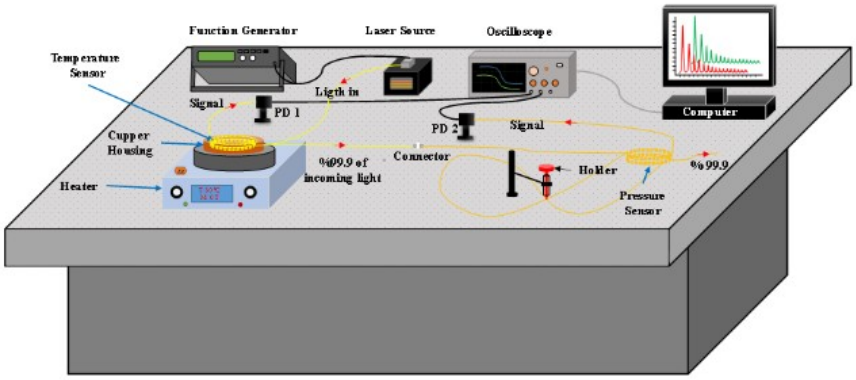

Figure 1. Schematic illustration of the system setup for the FLRDS sensor network.

In this study, a fiber loop ringdown spectroscopy (FLRDS) sensor network was developed by serially connecting two bare single-mode fiber (SMF) loops for simultaneous temperature and pressure sensing. One unmodified SMF loop embedded in a copper housing was used for temperature measurement, while the second loop incorporated a fiber cross-point for pressure detection, enabling a simple and flexible sensor design. The proposed system offers high sensitivity, rapid response, and real-time monitoring within a low-cost and portable architecture. Unlike conventional optical sensors, it does not require optical spectrum analyzers, optical time-domain reflectometers, fiber Bragg gratings, or specially fabricated sensing regions, thereby reducing system complexity and deployment cost. The sensor network achieved baseline stabilities of 0.21% for temperature sensing over 30–150 °C and 0.24% for pressure sensing up to 0.98×10^{6} Pa. Temperature sensitivities on the order of 10^{-1} μs/°C and pressure sensitivities on the order of μs per 10^{5} Pa confirm the robustness of the system for multiparameter sensing. Owing to its scalability, simplicity, and time-domain interrogation, the proposed FLRDS-based

SMF network is well suited for long-term monitoring in healthcare, infrastructure, industrial, environmental, and smart transportation applications, with strong potential for integration with nano-engineered fiber coatings and functional nanomaterials. A light beam trapped into the fiber loop takes many round trips inside the fiber loop until it decays. Due to a decrease in the optical loss, the intensity of the light beam decreases in every single turn in the loop. Hence, the intensity of signals sent to the photodetector decreases at each round trip. The change in intensity of the pulse I can be written as [33, 50]:

$$I = I_0 \cdot e^{-\frac{A \cdot c \cdot t}{n \cdot L}} \quad (1)$$

where: I is the intensity at time t, I_0 is the intensity of initial beam, A is the transmission loss in total for the trapped beam in the fiber loop per round trip (dimensionless, in terms of a ratio), c is the speed of light in vacuum, n is the average refractive index of the fiber and L is the total length of the fiber loop.

The time it takes for the intensity I to decay from I_0 to a lower value (I_0/e) is called the ringdown time (RDT), denoted as τ_0, and is given by equation (2) [33, 50]:

$$\tau_0 = \frac{n \cdot L}{c \cdot A} \quad (2)$$

When an external process such as a change in temperature or pressure occurs on or around the sensor head region, it induces an additional optical loss denoted by (B). As a result, τ of the system changes and is given by equation (3) [33,50]:

$$\tau = \frac{n \cdot L}{c \cdot (A + B)} \quad (3)$$

In a fiber loop ringdown spectroscopy (FLRDS) system, the overall transmission loss remains constant under normal conditions, as it is determined by the intrinsic properties of the fiber loop. These include transmission and absorption losses, as well as insertion losses at the couplers. However, when an external parameter such as temperature, pressure, or strain changes in the vicinity of the sensor head, an additional optical loss, denoted as B, is introduced. This added loss modifies the ringdown time of the system and can be expressed using equations (2) and (3) as [33,50]:

$$B = \frac{n \cdot L}{c}\left(\frac{1}{\tau} - \frac{1}{\tau_0}\right) \quad (4)$$

When a sensing event (e.g., temperature variation or applied pressure/strain) occurs at the sensor head, the total optical loss of the system changes. This change can be quantified by comparing the RDTs before and after the event. The difference in RDTs corresponds to the additional optical loss B, which arises from scattering in the evanescent field (EF), induced by the external perturbation. Since the EF is sensitive to environmental changes, the measured RDTs will differ accordingly.

The minimum detectable optical loss, a critical parameter for defining the detection sensitivity of the system, can be derived by modifying equation (4), as detailed in [51, 52]:

$$B = \left(\frac{t_r}{\tau_0}\right)\left(\frac{\Delta\tau}{\tau}\right) = \frac{1}{m}\frac{\Delta\tau}{\tau} \quad (5)$$

where $\Delta\tau = \tau_0 - \tau$, m is the number of turns of the fiber in the loop, and t_r is (n·L/c) which is the time taken for a single round trip of a light pulse in the loop. Therefore, the expression for the lowest detectable optical loss B_{min}, considering baseline noise, becomes [51, 52]:

$$B_{min} = \left(\frac{t_r}{\tau_0}\right)\left(\frac{\sigma}{\tau_{ave}}\right) = \frac{1}{m}\left(\frac{\sigma}{\tau_{ave}}\right) \quad (6)$$

where: σ is the standard deviation of the RDT, representing the 1-σ noise level; (σ/τ_{ave}) is in the order of $\sim 10^{-3}$; and an average level of the lowest detectable $(\Delta I/I_0)$ for an intensity-based systems, which is called the baseline noise of ringdown. This value characterizes the baseline noise of the ringdown signal [51,52]. For example, t_r and m are theoretically calculated to be 587.55 ns and 16, respectively, for a 120 m loop. For a 45 m loop, the values t_r and m are 220.33 ns and 17, respectively. Additional information regarding baseline stability can be found in [33, 53–56].

A small temperature variation δT induces a change δn in the refractive index of the fiber loop. This change perturbs the optical path and introduces a loss proportional to $(\alpha_t \cdot \delta T)$, where α_t is the temperature-dependent loss coefficient. As a result, equation (2) can be expressed as [33,53–56]:

$$\tau = \frac{(n+\delta n)\cdot L}{c\cdot(A+\alpha_t\cdot\delta T)} \quad (7)$$

Given that the refractive index change δn is small compared to the base refractive index n, it can be approximated as $n \approx n+\delta n$. This allows equation (7) to be simplified as [33,53–56]:

$$\tau = \frac{n\cdot L}{c\cdot(A+\alpha_t\cdot\delta T)} \quad (8)$$

If the optical loss due to δT is much lower than the total optical loss of the system $(\alpha_t \cdot \delta T \ll A)$, equation (8) can be written as [33,53–56]:

$$\tau = \frac{n\cdot L}{c\cdot A}\left(1+\frac{\alpha_t\cdot\delta T}{A}\right)^{-1} = \tau_0\cdot\left(1-\frac{\alpha_t\cdot\delta T}{A}\right) \quad (9)$$

Equation (9) shows that the ringdown time τ is linear dependent on the temperature, confirming that the RDT is sensitive to small temperature changes.

In the case of pressure sensing, when a force is applied to the sensor, pressure P = (F/S), where F is the applied force and S is the contact area through which the force is exerted on the fiber loop. This induces a force-perturbed B optical loss, defined as $B = \varepsilon_f \cdot L \cdot F$, where ε_f is the force-perturbed loss coefficient, L is the fiber length, and F is the applied force. Assuming $B \ll A$, equation (4) can be rewritten with B substituted as [30]:

$$\left(\frac{1}{\tau}-\frac{1}{\tau_0}\right) = \frac{c\cdot B}{n\cdot L} = \gamma\cdot P \quad (10)$$

where: γ is a constant.

Equation (10) confirms that the ringdown time τ has an inverse relationship with the applied pressure. Therefore, as the pressure increases, the RDT decreases proportionally, enabling pressure measurement through optical loss variations [30].

3. Results and discussions

Figure 2 shows continuous monitoring of Ringdown times (RDT) for two different fiber loops of

temperature and pressure sensor systems with 118±2 m and 43±2 m loop lengths, respectively. The temperature sensor was embedded into a copper housing to test in the range of temperature 30 ÷150 °C with 30 °C steps. Baseline stability is a critical factor in fiber loop ringdown spectroscopy (FLRDS) systems, as it directly determines the minimum detectable optical loss and thus the overall sensing sensitivity. In the present work, baseline stability was evaluated by recording one hundred consecutive ringdown time (RDT) data points with 128-time averaging for both temperature and pressure sensing loops under steady-state conditions. The obtained baseline stabilities were 0.21% for the temperature sensing loop and 0.24% for the pressure sensing loop, calculated based on one standard deviation. These low baseline instability values represent a significant improvement compared to many previously reported FLRDS-based sensing systems and can be attributed to the simplified optical architecture, the elimination of wavelength-domain components, and the mechanical stabilization of the fiber loops. The achieved baseline stability provides a solid foundation for reliable multi-parameter sensing with high sensitivity and long-term measurement robustness.

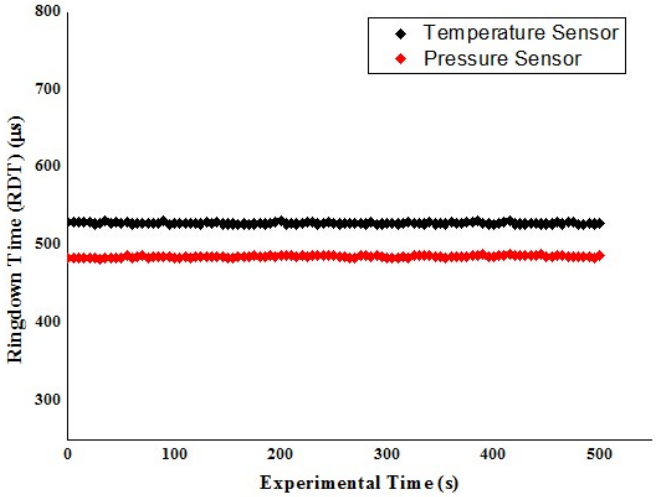

Figure 2. The stabilities of the baseline for the FLRDS temperature and pressure sensing systems.

Figure 3a shows temperature and pressure sensing data set when the first fiber loop with 118±2 m length was employed. For the temperature monitoring, the housing temperature was adjusted to 30 °C and waited until equilibrium of the housing. Furthermore, the temperature was increased until 150 °C with 30 °C steps at each 5 min. The monitored RDT was 501±0.5 μs when the fiber loop was in the housing and the temperature was set to 30 °C. As the temperature increased to 150 °C, the RDT was increased to 518±0.5 μs. According to Equation (9), an increase in the RDT must cause an increase in the temperature. Increase in the RDT is not only due to temperature increase, but also increase in the refractive index. Although temperature increments of 30 °C were applied in this study, this choice was made to initially validate the linearity, stability, and robustness of the proposed FLRDS-based sensor over a wide temperature range. The achieved low baseline instability (0.21%) and the linear dependence of the ringdown time on temperature, as described by Equations (7)–(9), indicate that the system is inherently capable of resolving smaller temperature variations. In principle, temperature steps of 10 °C or lower are detectable within the noise limit of the system. Further investigations employing finer temperature intervals will be conducted in future work to quantitatively determine the minimum detectable temperature change.

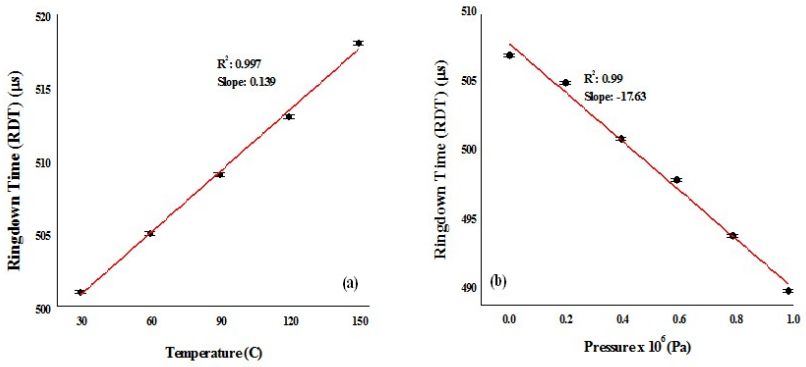

Figure 3. Temperature and pressure measurements with the FLRDS sensing system including 118±2 m fiber loop.

Rana et. al. [57] was studied temperature effect on the RI and showed that an increase in the temperature results in an increase in the RI. The data in Figure 3a follows a linear upward trend for the specified range of temperature with R^2 of 0.997.

The temperature response of the 118 ± 2 m fiber loop exhibits a clear linear increase in ringdown time with increasing temperature, confirming the theoretical prediction described in Equation (9). The obtained linearity (R^2 = 0.997) demonstrates the robustness and repeatability of the proposed FLRDS-based temperature sensor. For the pressure sensing, the cross-point sensor area was created and a lightweight holder was setup on it similar to shown in Figure 1, the RDT of the system was 507±0.5 µs. This value was accepted as the reference data because the weight of the holder barely created an optical loss and the RDT of the system might be changed. Applied pressure resulted in a monotonic decrease in ringdown time due to pressure-induced optical loss at the fiber cross-point. The observed linear response (R^2 = 0.99) confirms the suitability of the proposed configuration for quantitative pressure sensing. The monitored RDT was linearly decreased by adding weights up to 490±0.5 µs. This is consistent with the pressure sensing study by Wang and Scherrer [30] so that increasing pressure on the fiber will create extra optical loss, resulting a decrease in the RDT. Therefore, the data in Figure 3b follows a linear downward trend for the specified pressure range with R^2 of 0.99. The pressure range of 0–0.98×10^6 Pa was selected to demonstrate the linearity and repeatability of the proposed cross-point-based pressure sensor under controlled laboratory conditions. Owing to the highly localized interaction area at the fiber cross-point and the achieved baseline stability of 0.24%, the system is inherently capable of detecting smaller pressure variations. Extension of the pressure range or operation at lower pressure levels can be readily achieved by adjusting the applied load or the contact geometry, depending on the targeted application. Similarly, the second fiber loop with length 43±2 m was individually tested for the temperature and pressure sensing. The loop was confined in the sealed copper housing and temperature was increased with 30 °C steps in the range of 30 °C and 150 °C, resulted increasing the RDT from 481±0.5 µs to 495±0.5 µs, respectively. The same upward trend was observed as shown in Figure 4a with R^2 of 0.992. This result further confirms that smaller temperature steps can be resolved due to the high linearity and low baseline noise of the FLRDS system. A cross-point was created and pressure applied with the range of 0 to 0.98×10^6 Pa. A similar downward trend was observed as shown in Figure 4b with R^2 of 0.986. This behavior confirms the scalability of the pressure sensing mechanism with respect to both applied load and fiber loop length. Comparison of Figures 3 and 4 reveals that longer fiber loops provide higher temperature sensitivity, whereas shorter loops exhibit faster response and improved linearity.

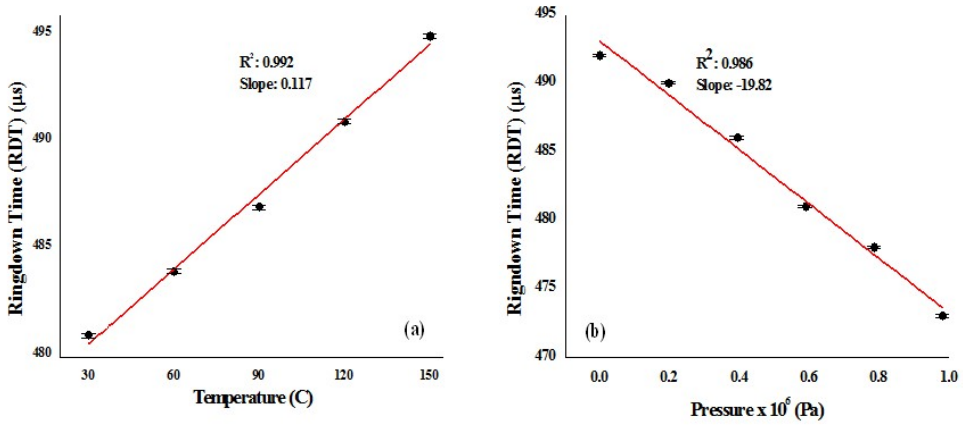

Figure 4. Temperature and pressure measurements with the FLRDS sensing system including 43±2 m fiber loop.

This trade-off confirms the critical role of fiber loop length in optimizing FLRDS sensor performance. From the linear fittings presented in Figures 3 and 4, the temperature sensitivity of the 118 ± 2 m fiber loop is approximately 0.14 µs/°C, while the sensitivity of the 43 ± 2 m loop is approximately 0.09 µs/°C. For pressure sensing, sensitivities on the order of several microseconds per 10^5 Pa were obtained, depending on the fiber loop length. These sensitivity values, combined with baseline noise levels on the order of 10^{-3}, confirm the high sensitivity of the proposed FLRDS sensor network.

Table 1 compares the performance of the proposed sensor network with representative FLRDS-based and fiber-optic temperature/pressure sensors reported in the literature. Compared to systems employing FBGs, interferometric structures, or optical spectrum analyzers, the present work achieves comparable sensitivity while significantly reducing system complexity and cost. In particular, the achieved baseline stability (≤0.24%) is among the lowest reported for FLRDS-based multiparameter sensors, which directly contributes to enhanced detection limits and long-term reliability. To evaluate repeatability, multiple measurement cycles were performed under identical experimental conditions. The variation in the extracted ringdown times was within the baseline noise level, indicating good repeatability and measurement reliability of the proposed sensor network.

Table 1. Quantitative comparison of the proposed FLRDS-based sensor network with representative fiber-optic temperature and pressure sensors

Reference	**Sensing technique**	**Measured parameters**	**Sensing element**	**Interrogation method**	**Sensitivity**	**Baseline stability / noise**	**Need OSA / complex optics**	**System complexity**
Chang et al. [43]	Fiber loop + FBG	Temperature, displacement	FBG + SMF loop	Wavelength-domain	~10 pm/°C	Not reported	Yes (OSA)	High
Jin et al. [44]	Birefringent SMF loop mirror	Temperature	Pressure-induced SMF	Polarization / wavelength	~0.02 nm/°C	Moderate	Yes (OSA)	High
Wang & Scherrer [30]	FLRDS	Pressure	Modified SMF region	Time-domain (RDT)	µs per 10^5 Pa	~0.5–1%	No	Medium
Chen et al. [41]	FLRDS + interferometry	Temperature	Interferometric structure	Frequency-shifted	µs/°C	~0.4%	Partial	Medium–High
Kaya et al. [49]	FLRDS	Temperature	Bare SMF loop	Time-domain (RDT)	~0.1 µs/°C	~0.3%	No	Low
This work	FLRDS	Temperature &	Bare SMF loops +	Time-domain	~0.14	0.21% (T)	No	Low

	sensor network	Pressure	cross-point	(RDT)	μs/°C (T) μs per 10^5 Pa (P)	0.24% (P)		

Among these parameters, baseline stability is particularly critical in FLRDS systems, as it directly determines the minimum detectable optical loss and thus the practical sensing resolution. As summarized in Table 1, the proposed FLRDS-based sensor network distinguishes itself from previously reported fiber-optic temperature and pressure sensors by combining multi-parameter capability, low baseline noise, and a simplified system architecture. Unlike FBG- or interferometer-based systems that require wavelength-domain interrogation and optical spectrum analyzers, the present approach relies solely on time-domain ringdown detection using bare single-mode fiber loops. The achieved baseline stabilities of 0.21% and 0.24% are among the lowest reported for FLRDS-based multiparameter sensors, directly contributing to enhanced detection sensitivity and long-term measurement reliability. These advantages make the proposed sensor network particularly attractive for scalable and nano-integrated sensing applications. While the slopes were decreasing with decreasing fiber loop length, the R^2 values were increasing. This observation further supports the rationale behind the selected loop lengths, as it highlights the direct influence of fiber length on sensitivity, response rate, and measurement linearity in FLRDS-based sensing systems. The longer the fiber loop is, the slower the increase in the RDT is for the temperature monitoring and the slower the decrease in the RDT is for the pressure sensing. This behavior is consistent with our previous findings [33] as a strain sensor was created and a strain created on the sensor head from the different points. Therefore, changes in slopes and R^2 values can be attributed to the ratio of the optical loss change. The smaller the fiber loop, the faster the optical loss change. Following, the both loops were connected in series and performed as the temperature sensor (118±2 m loop) and the pressure sensor (43±2 m loop) simultaneously.

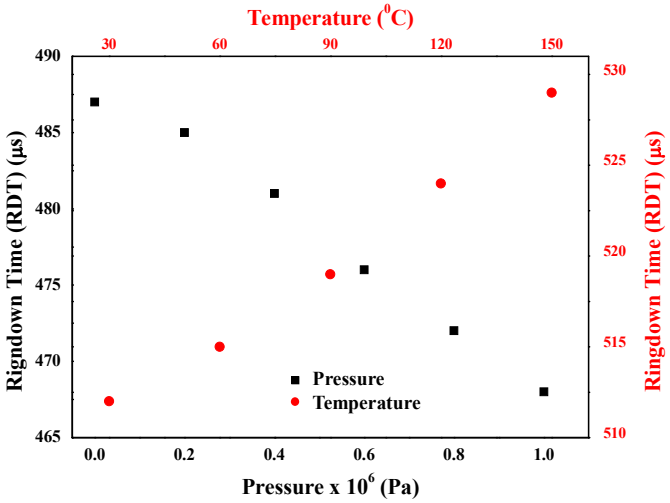

Figure 5. Data set from the FLRDS sensor network designed by temperature and pressure sensors.

Figure 5 shows the data set of the sensors. While the temperature sensor was in the housing at 30 °C, the RDT of the system was 512±0.5 μs. The RDT of the pressure sensor was recorded as 487±0.5 μs when there is no pressure on the cross-point. The similar trend was observed in the sensor network study when the temperature was changed from 30 °C to 150 °C with 30 °C steps and the pressure was increased from 0 to 0.98×10^6 Pa. As a result, this study focused on an innovative application of FLRDS sensor network setup utilizing bare SMF loops, without incorporating any additional optical components such as an OSA, an OTDR, or specialized sensing regions such as an air gap or a FBG. The FLRDS sensor

network was configured using two identical loops of different lengths for temperature and pressure sensing. For temperature sensing, unlike previous studies in the literature, a bare SMF loop was directly used as the sensing element. For pressure sensing, a fiber cross-point configuration was designed to minimize the contact area between the holder tip and the fiber, enhancing sensitivity. Furthermore, the number of sensing elements can be increased by connecting multiple loops in series or parallel configurations. The promising results demonstrated that the FLRDS sensor network holds strong potential for simultaneous multi-parameter sensing, offering high sensitivity, fast response, and real-time monitoring capabilities.

4. Conclusions

In this study, a novel fiber loop ringdown spectroscopy (FLRDS) sensor network was developed by serially connecting two bare single-mode fiber (SMF) loops to enable simultaneous temperature and pressure sensing. One unmodified SMF loop embedded in a copper housing was used for temperature measurement, while the second loop incorporated a fiber cross-point for pressure detection, demonstrating an efficient and flexible sensor design. The proposed system provides high sensitivity, fast response, and real-time monitoring while maintaining a simple, low-cost, and portable architecture. Unlike conventional optical sensor systems, it does not require optical spectrum analyzers, optical time-domain reflectometers, fiber Bragg gratings, or specially fabricated sensing regions, significantly reducing system complexity and deployment cost. The sensor network achieved excellent baseline stability of 0.21% for temperature sensing in the range of 30–150 °C and 0.24% for pressure sensing up to 0.98×10^{6} Pa. Temperature sensitivities on the order of 10^{-1} μs/°C and pressure sensitivities on the order of μs per 10^{5} Pa were obtained, confirming the robustness and reliability of the system for multiparameter sensing. Owing to its scalability, simplicity, and time-domain interrogation, the proposed FLRDS-based SMF network is highly suitable for long-term monitoring applications in healthcare, infrastructure, industrial processes, environmental sensing, and smart transportation, and shows strong potential for future integration with nano-engineered fiber coatings and functional nanomaterials.

Acknowledgements: The research was partially supported by Eskisehir Osmangazi University Scientific Research Project Department with the project code FHD-2023-2631.

Funding: The work received no funding.

Data Availability Statement: The data that support the findings of this study are available from the corresponding authors upon reasonable request.

Competing interests: The authors declare that they have no competing interests.

References

[1] Y.J. Rao, and D.A. Jackson. (1996). Recent Progress in Fibre Optic Low-Coherence Interferometry. Measurement Science and Technology 7: 981–999. https://doi.org/10.1088/0957-0233/7/7/001

[2] Y.J. Rao. (1997). Review Article: In-Fiber Bragg Grating Sensors. Measurement Science and Technology 8: 355–375. doi:10.1088/0957-0233/8/4/002

[3] B. Culshaw, and A. Kersey. (2008). Fiber-Optic Sensing: A Historical Perspective. Journal of Lightwave Technology 26: 1064–1078. https://doi.org/10.1109/JLT.0082.921915

[4] Ș. Țălu, H.T. Phuong, Dung N.T. Dung, (2025), Influence of initial pH on the ultrasonic synthesis of nanosilica from liquid glass, Journal of Nanomaterials and Applications, 1(1), 43–52. https://doi.org/10.65273/hhit.jna.2025.1.1.43-52

[5] Y.J. Rao. (2006). Recent Progress in Fiber-Optic Extrinsic Fabry–Perot Interferometric Sensors. Optical

Fiber Technology 12: 227–237. https://doi.org/10.1016/j.yofte.2006.03.004

[6] Y. Zhang, Y. Li, T. Wei, X. Lan, Y. Huang, G. Chen, and H. Xiao. (2010). Fringe Visibility Enhanced Extrinsic Fabry–Perot Interferometer Using a Graded Index Fiber Collimator. IEEE Photonics Journal 2: 469–481. https://doi.org/10.1109/JPHOT.2010.2049833

[7] T. Zhu, D. Wu, M. Liu, and D. W. Duan. (2012). In-Line Fiber Optic Interferometric Sensors in Single-Mode Fibers." Sensors 12: 10430–10449. https://doi.org/10.3390/s120810430

[8] Tripathi, S. M., A. Kumar, R. K. Varshney, Y. B. P. Kumar, E. Marin, and J. P. Meunier. "Strain and Temperature Sensing Characteristics of Single-Mode–Multimode–Single-Mode Structures." Journal of Lightwave Technology 27 (2009): 2348–2356. https://doi.org/10.1109/JLT.2008.2008820

[9] Wu, C., H. Y. Fu, K. K. Qureshi, B. Guan, and H. Y. Tam. "High-Pressure and High-Temperature Characteristics of a Fabry–Perot Interferometer Based on Photonic Crystal Fiber." Optics Letters 36 (2011): 412–414. https://opg.optica.org/ol/abstract.cfm?URI=ol-36-3-412

[10] Choi, H. Y., K. S. Park, S. J. Park, U. C. Paek, B. H. Lee, and E. S. Choi. "Miniature Fiber-Optic High Temperature Sensor Based on a Hybrid Structured Fabry–Perot Interferometer." Optics Letters 33 (2008): 2455–2457. https://doi.org/10.1364/OL.33.002455

[11] Pinto, A. M. R., O. Frazao, J. L. Santos, M. Lopez-Amo, J. Kobelke, and K. Schuster. "Interrogation of a Suspended-Core Fabry–Perot Temperature Sensor Through a Dual Wavelength Raman Fiber Laser." Journal of Lightwave Technology 28 (2010): 3149–3155. https://doi.org/10.1109/JLT.2010.2078490

[12] Rao, Y. J., M. Deng, D. W. Duan, X. C. Yang, T. Zhu, and G. H. Cheng. "Micro Fabry–Perot Interferometers in Silica Fibers Machined by Femtosecond Laser." Optics Express 15 (2007): 14123–14128. https://doi.org/10.1364/OE.15.014123

[13] Wei, T., Y. Han, Y. Li, H. Tsai, and H. Xiao. "Temperature-Insensitive Miniaturized Fiber Inline Fabry–Perot Interferometer for Highly Sensitive Refractive Index Measurement." Optics Express 16 (2008): 5764–5769. https://doi.org/10.1364/OE.16.005764

[14] Kou, J., J. Feng, L. Ye, F. Xu, and Y. Lu. "Miniaturized Fiber Taper Reflective Interferometer for High Temperature Measurement." Optics Express 18 (2010): 14245–14250.
https://doi.org/10.1364/OE.18.014245

[15] Japanese Standards Association. JIS Handbook: 33 Glass. Tokyo: Japanese Standards Association, 2010.

[16] Lau, K. S., K. H. Wong, and S. K. Yeung. "Fibre Optic Sensors for Laboratory Measurements." European Journal of Physics 13 (1992): 227–235. https://doi.org/10.1088/0143-0807/13/5/006

[17] Wang, G., Z. Wang, and R. O. Claus. "Two-Mode Elliptical Core Optical Fiber Sensors for Strain and Temperature Measurement." Smart Materials and Structures 4 (1995): 42–49.
https://doi.org/10.1088/0964-1726/4/1/007

[18] Li, K., Z. A. Zhou, and A. C. Liu. "A High Sensitive Fiber Bragg Grating Cryogenic Temperature Sensor." Chinese Optics Letters 7 (2009): 121–123.

[19] The Japan Society of Mechanical Engineers (JSME), ed. JSME Data Book: Heat Transfer, 5th ed. Tokyo: JSME, 2009.

[20] Martelli, C., P. Olivero, J. Canning, N. Groothoff, B. Gibson, and S. Huntington. "Micromachining Structured Optical Fibers Using Focused Ion Beam Milling." Optics Letters 32 (2007): 1575–1577. https://doi.org/10.1364/OL.32.001575

[21] Li, X., J. Pawlat, J. Liang, G. Xu, and T. Ueda. "Fabrication of Photonic Bandgap Fiber Gas Cell Using

Focused Ion Beam Cutting." Japanese Journal of Applied Physics 48 (2009): 06FK05–1–5. https://doi.org/10.1143/JJAP.48.06FK05

[22] Cavillon, M., P. D. Dragic, and J. Ballato. "Additivity of the Coefficient of Thermal Expansion in Silicate Optical Fibers." Optics Letters 42 (2017): 3650–3653. https://doi.org/10.1364/OL.42.003650

[23] Palik, E. D., ed. Handbook of Optical Constants of Solids. San Diego and London: Academic Press, 1997.

[24] Gao, H., Y. Jiang, Y. Cui, L. Zhang, J. Jia, and L. Jiang. "Investigation on the Thermo-Optic Coefficient of Silica Fiber Within a Wide Temperature Range." Journal of Lightwave Technology 36 (2018): 5881–5886. https://doi.org/10.1109/JLT.2018.2875941

[25] Adamovsky, G., S. F. Lyuksyutov, J. R. Mackey, B. M. Floyd, U. Abeywickrema, I. Fedin, and M. Rackaitis. "Peculiarities of Thermo-Optic Coefficient Under Different Temperature Regimes in Optical Fibers Containing Fiber Bragg Gratings." Optics Communications 285 (2012): 766–773. https://doi.org/10.1016/j.optcom.2011.10.084

[26] Li, L., D. Lv, M. Yang, L. Xiong, and J. Luo. "A IR-Femtosecond Laser Hybrid Sensor to Measure the Thermal Expansion and Thermo-Optical Coefficient of Silica-Based FBG at High Temperatures." Sensors 18 (2018): 359. https://doi.org/10.3390/s18020359

[27] Prod'Homme, L. "A New Approach to the Thermal Change in the Refractive Index of Glasses." Physics and Chemistry of Glasses 1 (1960): 119–122. https://doi.org/10.1002/lpor.202401086

[28] Talebian, E., and M. Talebian. "A General Review on the Derivation of Clausius–Mossotti Relation." Optik 124 (2013): 2324–2326. https://doi.org/10.1016/j.ijleo.2012.06.090

[29] Baak, T. "Thermal Coefficient of Refractive Index of Optical Glasses." Journal of the Optical Society of America 59 (1969): 851–857. https://doi.org/10.1364/JOSA.59.000851

[30] Wang, C., and S. T. Scherrer. "Fiber Loop Ringdown for Physical Sensor Development: Pressure Sensor." Applied Optics 43 (2004): 6458–6464. https://doi.org/10.1364/AO.43.006458

[31] Sahay, P., M. Kaya, and C. Wang. "Fiber Loop Ringdown Sensor for Potential Real-Time Monitoring of Cracks in Concrete Structures: An Exploratory Study." Sensors 13 (2012): 39–57. https://doi.org/10.3390/s130100039

[32] Ghimire, M., and C. Wang. "Highly Sensitive Fiber Loop Ringdown Strain Sensor with Low Temperature Sensitivity." Measurement Science and Technology 28 (2017): 105101. https://doi.org/10.1088/1361-6501/aa82a3

[33] Kaya, M., and O. Esentürk. "Study of Strain Measurement by Fiber Optic Sensors with a Sensitive Fiber Loop Ringdown Spectrometer." Optical Fiber Technology 54 (2020): 102070. https://doi.org/10.1016/j.yofte.2019.102070

[34] Wu, K., C. Zhao, B. Mao, J. Kang, H. Gong, H. Wang, and D. Wang. "Strain Sensor Based on FBG in Fiber Loop Ring Down System." Microwave and Optical Technology Letters 64 (2022): 1666–1670. https://doi.org/10.1002/mop.33316

[35] O'Dwyer, M. J., C. C. Ye, S. W. James, and R. P. Tatam. "Thermal Dependence of the Strain Response of Optical Fibre Bragg Gratings." Measurement Science and Technology 15 (2004): 1607–1613. https://doi.org/10.1088/0957-0233/15/8/031

[36] Jung, J., H. Nam, B. Lee, J. O. Byun, and N. S. Kim. "Fiber Bragg Grating Temperature Sensor with Controllable Sensitivity." Applied Optics 38 (1999): 2752–2754. https://doi.org/10.1364/AO.38.002752

[37] Tian, X., J. Shi, Y. Wang, Y. She, and L. Li. "Temperature Sensor Based on Fiber Bragg Grating

Combined with a Microwave Photonic-Assisted Fiber Loop Ring Down." Optics Express 30 (2022): 10110–10118. https://doi.org/10.1364/OE.450545

[38] Pal, S., T. K. Sun, T. V. Grattan, S. A. Wade, S. F. Collins, G. Baxter, W. B. Dussardier, and G. Monnom. "Strain-Independent Temperature Measurement Using a Type-I and Type-IIA Optical Fiber Bragg Grating Combination." Review of Scientific Instruments 75 (2004): 1327–1331.
https://doi.org/10.1063/1.1711155

[39] Nguyen, L. V., S. C. Warren-Smith, H. Ebendorff-Heidepriem, and T. M. Monro. "Interferometric High Temperature Sensor Using Suspended-Core Optical Fibers." Optics Express 24 (2016): 8967–8977. https://doi.org/10.1364/OE.24.008967

[40] Wang, C. "Fiber Ringdown Temperature Sensors." Optical Engineering 44 (2005): 030503. https://doi.org/10.1117/1.1869512

[41] Chen, J. X., C. F. Cheng, Y. W. Ou, W. J. Chen, M. M. Li, and I. Fang. "Fiber Loop Ringdown Temperature Sensor Using Frequency-Shifted Interferometry Technology." Journal of Optics 50 (2021): 621–628. https://doi.org/10.1007/s12596-021-00715-w

[42] Sun, B., T. Shen, and Y. Feng. "Fiber Loop Ringdown Magnetic Field and Temperature Sensing System Based on the Principle of Time-Division Multiplexing." Optik 147 (2017): 170–179.
https://doi.org/10.1016/j.ijleo.2017.08.093

[43] Chang, Y. T., C. T. Yen, Y. S. Wu, and H. S. Cheng. "Using a Fiber Loop and Fiber Bragg Grating as a Fiber Optic Sensor to Simultaneously Measure Temperature and Displacement." Sensors 13 (2013): 6542–6551. https://doi.org/10.3390/s130506542

[44] Jin, Y., C. C. Chan, Y. Zhang, X. Dong, and P. Zu. "Temperature Sensor Based on a Pressure-Induced Birefringent Single-Mode Fiber Loop Mirror." Measurement Science and Technology 21 (2010): 065204. https://doi.org/10.1088/0957-0233/21/6/065204

[45] Li, X., Y. Lu, and Z. Zhang. "Simultaneous Measurement of Temperature and Pressure Based on Forward Brillouin Scattering in Double-Coated Optical Fiber." Journal of Lightwave Technology 41 (2023): 5130–5137. https://doi.org/10.1109/JLT.2023.3249285

[46] Jiang, H., Z. Gu, K. Gao, Z. Li, Y. Yan, and J. Wu. "A High Sensitivity Sensor Based on Novel CLPFG with Wavelength and Intensity Modulation for Simultaneous Measurement of SRI and Temperature." Optical Fiber Technology 70 (2022): 102836. https://doi.org/10.1016/j.yofte.2022.102886

[47] Yang, T., Y. Wang, and X. Wang. "High-Precision Calibration for Strain and Temperature Sensitivities of Rayleigh-Scattering-Based DOFS at Cryogenic Temperatures." Cryogenics 124 (2022): 103481. https://doi.org/10.1016/j.cryogenics.2022.103481

[48] Wang, C., M. Kaya, P. Sahay, H. Alali, and R. Reese. "Fiber Optic Sensors and Sensor Networks Using a Time-Domain Sensing Scheme." Optics and Photonics Journal 3 (2013): 236–239.
https://doi.org/10.4236/opj.2013.32B055

[49] Kaya, B. M. "A Novel Single Mode Fiber Optic Temperature Sensor Combined with the FLRDS Technique." Physica Scripta 99 (2024): 095405. https://doi.org/10.1088/1402-4896/ad69cc

[50] Kaya, M., and O. Esentürk. "Highly Sensitive Fiber Optic Pressure Sensors for Wind Turbine Applications." Turkish Journal of Electrical Engineering and Computer Sciences 28 (2020): 2789–2796. https://doi.org/10.3906/elk-2003-69

[51] Wang, C. "Fiber Loop Ringdown—A Time-Domain Sensing Technique for Multi-Function Fiber Optic Sensor Platforms: Current Status and Design Perspectives." Sensors 9 (2009): 7595–7621.

https://doi.org/10.3390/s91007595

[52] Wang, C., and C. Herath. "High-Sensitivity Fiber-Loop Ringdown Evanescent-Field Index Sensors Using Single-Mode Fiber." Optics Letters 35 (2010): 1629–1631. https://doi.org/10.1364/OL.35.001629

[53] Kaya, M. "Fiber Optic Chemical Sensors for Water Testing by Using Fiber Loop Ringdown Spectroscopy Technique." Turkish Journal of Electrical Engineering and Computer Sciences 28 (2020): 2375–2384. https://doi.org/10.3906/elk-2005-39

[54] Kaya, M., C. Wang, and C. Wang. "Reproducibly Reversible Fiber Loop Ringdown Water Sensor Embedded in Concrete and Grout for Water Monitoring." Sensors and Actuators B: Chemical 176 (2013): 803–810. https://doi.org/10.1016/j.snb.2012.10.036

[55] Kaya, B. M., O. Esentürk, C. Asici, U. Sarac, G. Dindis, and M. C. Baykul. "Coating Effects on a Strain Sensor Durability and Sensitivity Using the Fiber Loop Ringdown Spectroscopy Technique." Physica Scripta 99 (2024): 055511. https://doi.org/10.1088/1402-4896/ad3784

[56] Kaya, B. M., S. Oz, and O. Esenturk. "Application of Fiber Loop Ringdown Spectroscopy Technique for a New Approach to Beta-Amyloid Monitoring for Alzheimer Disease's Early Detection." Biomedical Physics and Engineering Express 10 (2024): 035037. https://doi.org/10.1088/2057-1976/ad3f1f

[57] Rana, S., A. Fleming, H. Subbaraman, and N. Kandadai. "Real-Time Measurement of Parametric Influences on the Refractive Index and Length Change in Silica Fibers." Optics Express 30 (2022): 15659–15668. https://doi.org/10.1364/OE.450528